PROTON STRUCTURE FUNCTION DATA AND SEARCH FOR BFKL SIGNATURES AT HERA*

A. De Roeck

DESY, Notkestr.85, D-22607 Hamburg, Germany

We summarize data on the proton structure function $F_2(x, Q^2)$ from the electron-proton collider HERA. The kinematic range covered for $F_2(x, Q^2)$ measurements now reaches momentum transfers squared Q^2 between 1.5 GeV^2 and 5000 GeV^2 and Bjorken x between $3 \cdot 10^{-5}$ and 0.32. The new results represent an increase in statistics by a factor of ten with respect to the analysis of the 1993 data. The structure function is found to increase significantly with decreasing x, even in the lowest accessible Q^2 region. For $Q^2 > 5$ GeV^2, the data exhibit double asymptotic scaling. The data are well described by a Next-to-Leading Order QCD fit and the gluon density is extracted. Searches for BFKL signatures in the hadronic final states are briefly presented.

PACS numbers: 12.38.Qk

1. Introduction

On the 31st of May 1992 the first electron-proton (ep) collisions were observed in the H1 and ZEUS experiments at the newly commissioned high energy collider HERA, in Hamburg, Germany. HERA is the first electron-proton collider in the world: 26.7 GeV electrons collide on 820 GeV protons, yielding an ep centre of mass system (CMS) energy of 296 GeV. Already the results from the data collected during the first years by the experiments have given important new information on the structure of the proton, and on the QCD dynamics of the final state.

The basic process for deep inelastic scattering neutral current interactions at HERA is depicted in Fig. 1. The incoming electron interacts via the exchange of a γ, (and Z^0 at large momentum transfers) with a quark of the proton. This quark — often referred to as current quark — is kicked out of the proton, leaving behind a proton remnant. Both the current quark

* Presented at the Cracow Epiphany Conference on Proton Structure, Kraków, Poland, January 5–6, 1996.

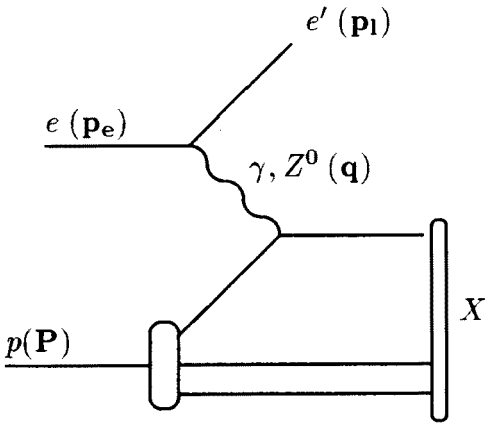

Fig. 1. Deep inelastic scattering at HERA for a neutral current process.

and the proton remnant hadronize into a hadronic final state, X in Fig. 1. The HERA experiments H1 and ZEUS measure both the scattered electron and the hadronic final state, apart from the hadrons close to the proton remnant which remain in the beam pipe.

At fixed CMS energy, $\sqrt{s}$, the kinematics of the inclusive ep scattering process, $ep \to eX$, is determined by two independent variables, conventionally chosen to be two of x, y and Q^2. These kinematical variables are defined as follows:

$$Q^2 = -q^2 = -(p_e - p_l)^2, \quad x = \frac{Q^2}{2P.q}, \quad y = \frac{P.q}{P.p_e},$$
$$W^2 = (q + P)^2 = Q^2 \frac{1-x}{x} + m_p{}^2, \tag{1}$$

where Q^2 is (minus) the four-momentum transfer squared, x the Bjorken-x, y the fraction of the electron energy transfered to the proton in the proton rest system, and W^2 the hadronic invariant mass squared of the system X. In the naïve quark parton model, *i.e.* the parton model with no QCD effects, the x variable measures the fraction of the proton momentum carried by the struck quark. In these definitions p_e, p_l and P denote the four-momenta of the incoming and scattered lepton and the incoming proton respectively, as indicated in Fig. 1.

One of the exciting open questions before the startup of HERA was the evolution of the structure of the proton at small values of Bjorken-x, say $x < 10^{-2}$. First results from HERA were shown in the spring of 1993, based on data collected in 1992, and demonstrated clearly an at the time somewhat unexpected and dramatic rise of the structure function with de-

creasing x (see [1]). The data immediately ruled out a Regge-based description at large Q^2, which is so successful for hadronic and photoproduction ($Q^2 = 0$) cross sections. The Regge model predicts a much slower rise with decreasing x than was observed in deep inelastic measurements of F_2. The observation generated great activity, particularly as application of the BFKL equation [2] had anticipated a singular $x^{-\lambda}$ growth with decreasing x. The traditional evolution equations to analyse in QCD the structure function data are the Altarelli–Parisi (DGLAP) [3] equations which evolve parton densities up in Q^2 from a set of starting distributions at a Q_0^2. At lowest order these evolution equations effectively resum the leading order $\alpha_s \log Q^2$ contributions. At small x however, large $\log 1/x$ terms are encountered which have to be resummed. When the first data on the strong rise of F_2 with decreasing x were shown, this rise was thought to be associated with resummation of those terms, as it arises from the BFKL equation.

Now two and a half years on, the measurements by H1 and ZEUS have improved remarkably as will be shown in the next sections. Furthermore, Next-to-Leading (NLO) order QCD DGLAP fits have been made on these data and these were found to give a good description of the data. The gluon distribution has been extracted at small x. New data on the contribution to F_2 which arises from charm production, $F_2^{c\bar{c}}$, become available. As it turns out, in order to demonstrate the effects of BFKL, F_2 may be too inclusive a measurement. Therefore, in addition, searches for effects of BFKL dynamics in the hadronic final states are being explored.

2. Structure function data from HERA

At this conference the HERA experiments presented results from the 1994 data taking period. During this period HERA collided 27.5 GeV positrons on 820 GeV protons, as opposed to the 26.7 GeV electrons in 1992 and 1993. The corresponding centre-of-mass energy of the ep collision is 300 GeV. The new F_2 results extend to larger Q^2 values due to a tenfold increase in statistics, compared to the data collected in 1993 (and about a factor of hundred increase with respect to the 1992 data). The data samples for F_2 analyses of the 1994 data contain between 2 and 3 pb^{-1}. Furthermore both the H1 and ZEUS experiments have made a special effort to obtain measurements at lower values of Q^2 so as to explore the region towards $Q^2 \to 0$. Values of Q^2 down to about 1 GeV^2 have been reached as a result of detector upgrades, operating HERA in a different collision mode called shifted interaction vertex mode, and by using events with initial state QED radiation from the incoming lepton. At the time of the Workshop all data were still preliminary, but by now have become final to a large extent [4, 5]. The ZEUS medium and high Q^2 data are still preliminary [6].

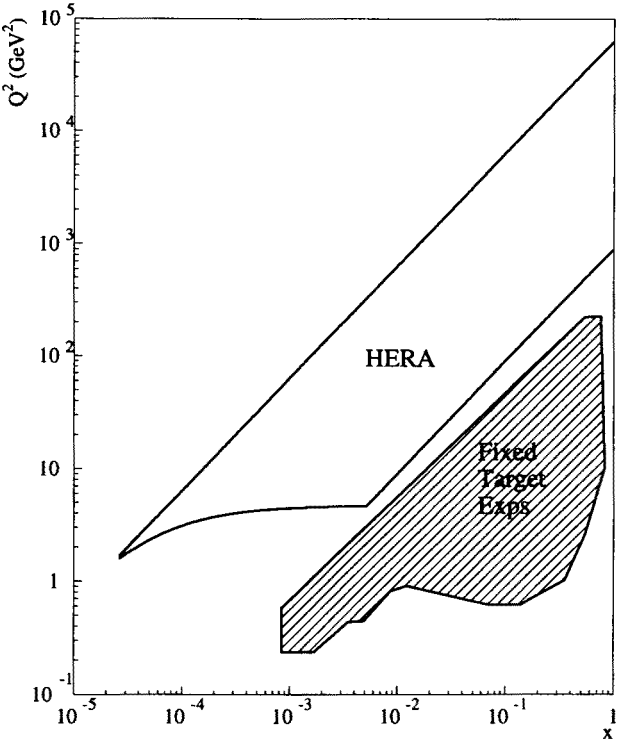

Fig. 2. The kinematical region covered by the HERA and fixed-target experiments.

The kinematic plane covered by HERA and the fixed-target measurements is shown in Fig. 2. Generally measurements at HERA can reach Q^2 (x) values two orders of magnitude larger (smaller) than those reached by fixed-target experiments. Fig. 2 shows that the two regions come almost within contact of each other and thus the continuity and normalization of the data can be checked. New upgrades of the HERA detectors will allow the exploration of even lower Q^2 in the future.

In the one-photon-exchange approximation, the differential electroproduction cross section is related to the structure function $F_2(x, Q^2)$ and the ratio $R(x, Q^2)$ of the cross sections for the longitudinally and transversally polarised virtual photons by

$$\frac{d^2\sigma}{dx dQ^2} = \frac{4\pi\alpha^2}{Q^4 x}\left[1 - y + \frac{y^2}{2(1+R)}\right] F_2(x, Q^2)\,. \tag{2}$$

The function $R(x, Q^2)$ has so far been measured only in fixed-target experiments, but even here information is scarce. For the HERA measurements R was calculated using the QCD relation [7] with the GRV structure function

parametrization (see below). Note that a 20% error on R corresponds to about a 2% uncertainty on F_2 at $y = 0.6$ for R of about 0.6. The effects due to Z boson exchange for neutral current interactions in the presently covered high Q^2 region for F_2 at HERA amount to a few percent only.

To determine the kinematical variables x and Q^2 for each event, we can use two out of four experimentally accessible quantities: the energy, E'_e, and angle, θ_e, of the scattered electron, and the energy, E_h, and average angle, θ_h, of the hadron flow. The electron method, is the method used so far in all fixed-target experiments. Here the basic formulae for Q^2 and y are

$$y_e = 1 - \frac{E'_e}{E_e} \sin^2 \frac{\theta_e}{2}, \quad Q^2_e = 4E'_e E_e \cos^2 \frac{\theta_e}{2} = \frac{E'^2_e \sin^2 \theta_e}{1 - y_e}. \tag{3}$$

The polar angle θ_e is defined with respect to the proton beam direction, referred to as "forward" region. It remains at HERA the most precise way to reconstruct Q^2 in the whole kinematic range. However at low y ($y < 0.1$) the measurement of x becomes poor and at large y ($y > 0.8$) the radiative corrections which need to be applied to the observed cross section to extract the Born cross section are very large. Kinematic variable determinations which combine electron and hadronic final state data bypass these difficulties and reach lower values in y. The ZEUS collaboration has used apart from the electron method, a method based on the angle of the electron and of the hadronic system [8]. A new method used by the H1 Collaboration [9, 10], called the Σ method, determines y and Q^2 from

$$y_\Sigma = \frac{\Sigma_h (E - P_z)_h}{(E - P_z)_e + \Sigma_h (E - P_z)_h}, \quad Q^2_\Sigma = \frac{E'^2_e \sin^2 \theta_e}{1 - y_\Sigma}, \tag{4}$$

where the sum runs over all hadrons in the numerator and over all hadrons plus the scattered electron in the denominator. In this method the energy of the incident electron in the interaction is reconstructed, which reduces drastically the sensitivity to the main radiative process. The resolution in x at low y is good enough to allow the H1 Collaboration to reach $y = 0.01$. The resolution at large y is worse but less sensitive to radiative corrections than when using only the measurement of the scattered electron. For precision measurements of the structure function the different methods are used to control the systematics of event smearing and radiative corrections. The comparison of these methods is discussed in [4]. For the final results H1 uses the electron method for $y > 0.15$ and the Σ method for $y < 0.15$. For the 1994 data analysis, ZEUS uses a method which is closely related to the Σ method [11]. Preliminary results showed that it may be possible to have a region of overlap with the fixed target data.

Due to the inevitable beam pipe hole for detectors at a collider, the scattered electron has to have a minimum angle to leave the beampipe and

be detected. From (3) it follows that this leads to a minimum requirement on Q^2, which is also visible in Fig. 2. To study whether F_2 still rises at lower values of Q^2, several ways to increase the acceptance for the low Q^2 region were explored.

The ZEUS detector was improved for electron detection around the beampipe by the addition of a scintillator strip detector on the face of the rear calorimeter. This allowed the detection of the scattered electron down to smaller angles (175.5° compared to 174° in 1993) with a large improvement of the angular resolution (2 mrad compared to 7 mrad in 1993). The detector was also used to make an event-by-event correction to the scattered electron energy arising from the energy loss in the inactive material prior to the calorimeter, thereby improving the energy resolution and reducing the energy scale uncertainty. Due to the large statistics the electron energy scale and angular shift uncertainty for the H1 results have been reduced to 1% and 1 mrad respectively. H1 could also — due to the excellent accelerator conditions at the end of the 1994 running period — make use of the most inner active elements of the calorimeter, and increase its low scattering angle acceptance from 173° to 174°. In 1993 H1 initiated a pilot project to shift the interaction vertex of the collisions towards the forward (proton) region. They demonstrated that collisions produced at a position shifted by about 70 cm downstream of the detector could still be used for F_2 analysis, and allowed an increase in the acceptance from 8.5 GeV^2 to 4.5 GeV^2 for the 1993 data. In 1994 about 10 times more data were accumulated using this method, and results have been shown by both experiments.

Another way to access low Q^2 is by using a sample of deep inelastic events with an energetic photon (*e.g.* $E_\gamma > 4$ GeV) emitted collinear with the incident electron. These radiative events can be interpreted as deep inelastic scattering events with a reduced incident energy $E_r = E_e - E_\gamma$ which can be reconstructed through the detection of the radiated photon in the small angle photon tagger of the luminosity system of the experiments. When using the electron method, the "true" kinematic variables y_t and Q_t^2 for such an ep collision are obtained by replacing in (3) the nominal beam energy by the reduced energy E_r. Both experiments have shown data using this process [4, 5].

In summary, compared to the previous analyses, the F_2 measurement has been extended to lower and higher Q^2 (from 4.5 – 1600 GeV^2 to 1.5 – 5000 GeV^2), and to lower and higher x (from $1.8 \times 10^{-4} - 0.13$ to $3 \times 10^{-5} - 0.32$). The result is shown in Fig. 3 as a function of x and in Fig. 4 as a function of Q^2. The error bars of the data are now reduced to the 5% to 10% level (except at high and very low Q^2). The normalization uncertainty has been reduced to 1.5% (2.5%) for H1 (ZEUS). The rise of

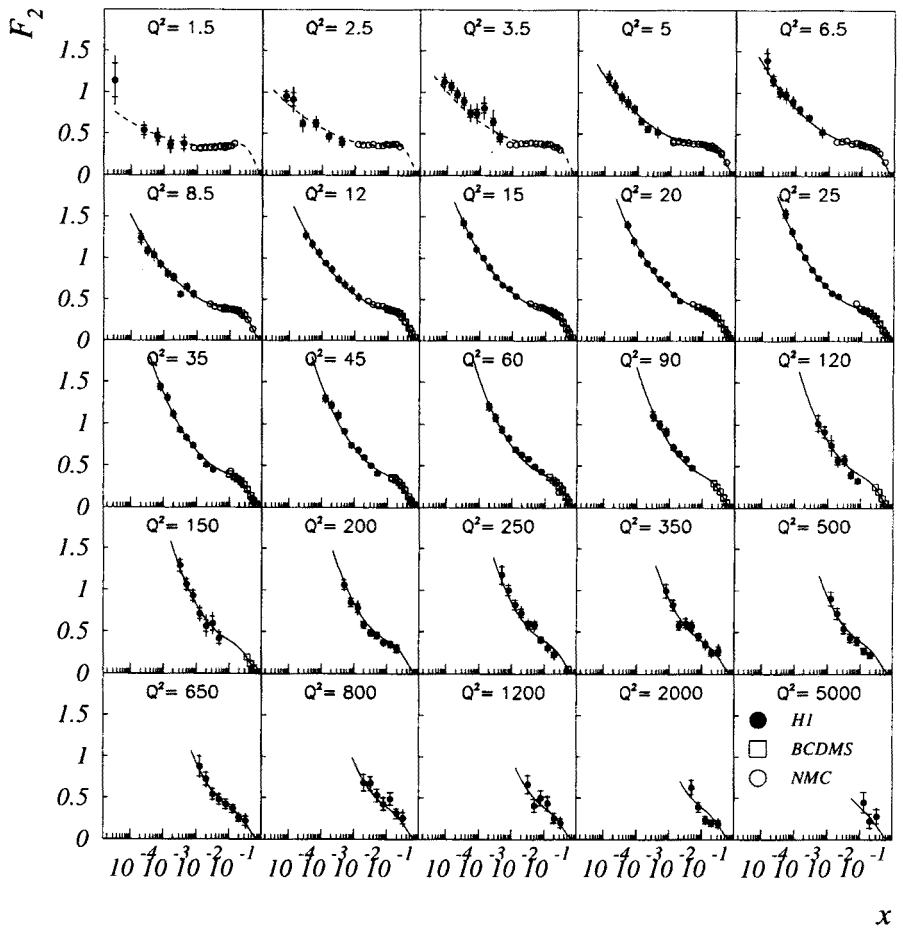

Fig. 3. Measurement of the structure function $F_2(x, Q^2)$ as function of x. The closed circles are H1 data, the open symbols are data from NMC [12] and BCDMS [13]. The inner error bar is the statistical error. The full error bar represents the statistical and systematic errors added in quadrature disregarding the luminosity errors. The curves represent the NLO QCD fit, discussed in Section 3.

F_2 with decreasing x, is confirmed with impressive precision. This rise continues, albeit less strongly than at higher Q^2, in the region of the lowest Q^2 available. The data show a smooth continuation from the fixed target (NMC/BCDMS/E665) to the HERA data. Scaling violations are clearly seen in the Fig. 4 and will be interpreted in terms of QCD in the next Section.

The persistent rise of F_2 at low x for small Q^2 indicates that the photoproduction regime has not been reached yet. This can be seen clearly in Fig. 5 which shows the strong rise of F_2 as a function of W, the invariant

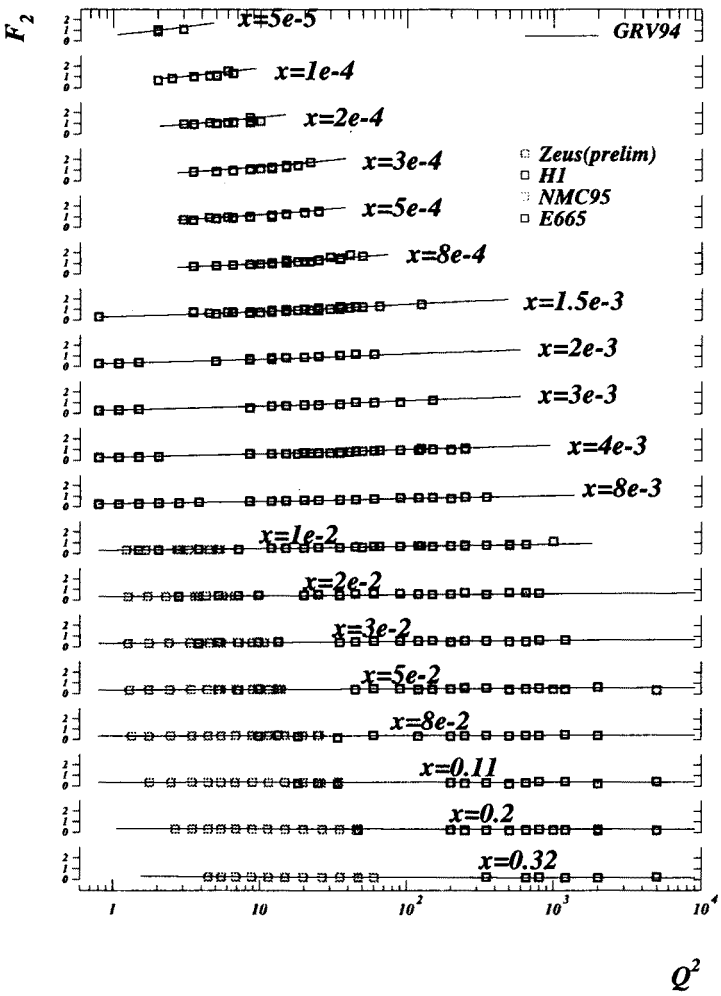

Fig. 4. Measurement of the structure function $F_2(x, Q^2)$ as function of Q^2 for the H1, ZEUS, NMC and E665 [14] experiments. The curve is the prediction of the GRV parton distributions.

mass of the $\gamma^* p$ system (at low x, $W \simeq \sqrt{Q^2/x}$). F_2 is related to the total cross section of the proton-virtual photon interaction $\sigma_{tot}(\gamma^* p)$ via

$$\sigma_{\rm tot}(\gamma^* p) \simeq \frac{4\pi^2 \alpha}{Q^2} F_2(W, Q^2)\,. \tag{5}$$

The F_2 growth can be contrasted with the weak rise with W of the total real photoproduction cross section in the same range of W, as shown in Fig. 5.

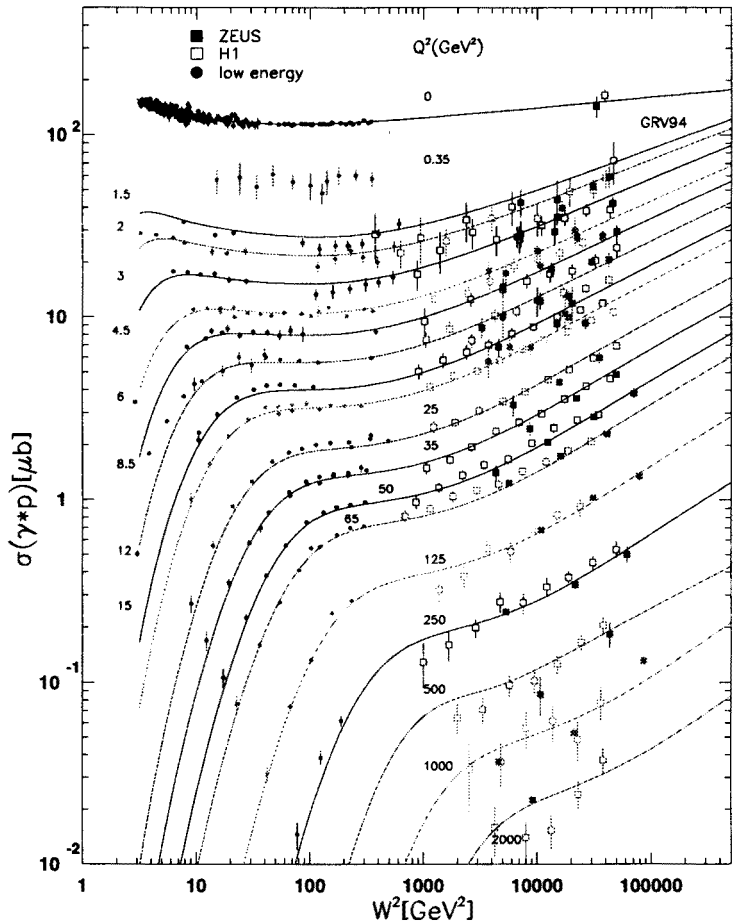

Fig. 5. Measurement of the proton structure function $F_2(W, Q^2)$ as function of W^2. Also data at $Q^2 = 0$ are shown. The curves are the GRV parametrization (see text).

The different behaviour for $Q^2 = 0$ and data at a finite small Q^2 remains one of the interesting questions to be studied at HERA.

3. Discussion of the F_2 data and QCD analysis

To emphasize the rise of F_2 at low Q^2, data from the eight lowest Q^2 bins are shown and compared with recent F_2 parametrizations in Fig. 6. It demonstrates that the rise of F_2 towards low x is also present in the low Q^2 region. The measurement is in good agreement with recent data from fixed-target experiments E665 and NMC at higher x values. The curves represent

DGLAP QCD inspired predictions (GRV [15], MRS [16] and CTEQ [17]) and two Regge inspired predictions (DOLA [18] and CKMT [19], the latter is not QCD evolved for this figure). The Regge inspired predictions, shown only for the lowest Q^2 bins, are generally below the data. These models were already disfavoured by the early HERA F_2 data for the region $Q^2 > 5$ GeV^2. It turns out with the new low Q^2 data that at least the DOLA model disagrees with the data down to $Q^2 \sim 1$ GeV^2.

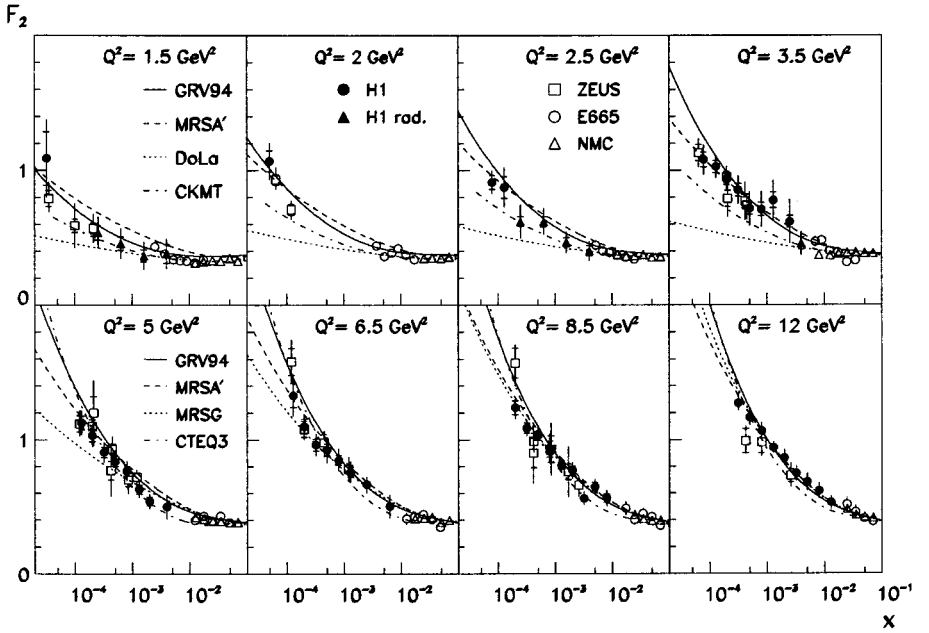

Fig. 6. Measurement of the proton structure function $F_2(x, Q^2)$ in the low Q^2 region by H1 (closed circles: non-radiative events; closed triangles: radiative events), together with results from the ZEUS (open squares), E665 (open points) and NMC (open triangles) experiments. Different parametrizations for F_2 are compared to the data. The DOLA and CKMT curves are only shown for the upper row of Q^2 bins; CTEQ3M and MRSG are shown for the lower row; GRV and MRSA′ are shown for the full Q^2 range. The Q^2 values of the ZEUS data shown for the bins $Q^2 = 3.5$, 5 and 6.5 GeV^2 are measurements at 3.0, 4.5 and 6 GeV^2 respectively.

The MRS and CTEQ distributions result from global DGLAP fits of data, and assume a $x^{-\lambda}$ behaviour for the seaquark and gluon densities, for $x \to 0$, at some scale Q_0^2 of typically a few GeV^2. The agreement between data and fit (which did not include the 1994 F_2 data) shows already that generally the DGLAP evolution equations are able to account for the rise of F_2. The predictive power in new kinematical regions of such types

of fits is however limited. The GRV calculation assumes that all parton distributions at very low $Q_0^2 = 0.34$ GeV^2 have a valence like shape, *i.e.* vanish for $x \to 0$. Assuming that the DGLAP equations can be used to evolve the parton distributions from this low Q_0^2 scale to larger Q^2 values, they predicted that the structure function F_2 should rise towards low x even for low values of $Q^2 \sim 1$ GeV^2. The determination of the shape parameters of the distributions at the starting scale uses only data from fixed target experiments and not much freedom is left for further adjustments in the kinematic range of the HERA data. The agreement with the HERA data is impressively good at this stage of the precision. Again it demonstrates that the DGLAP evolution equations can account for the rise of F_2 at small x.

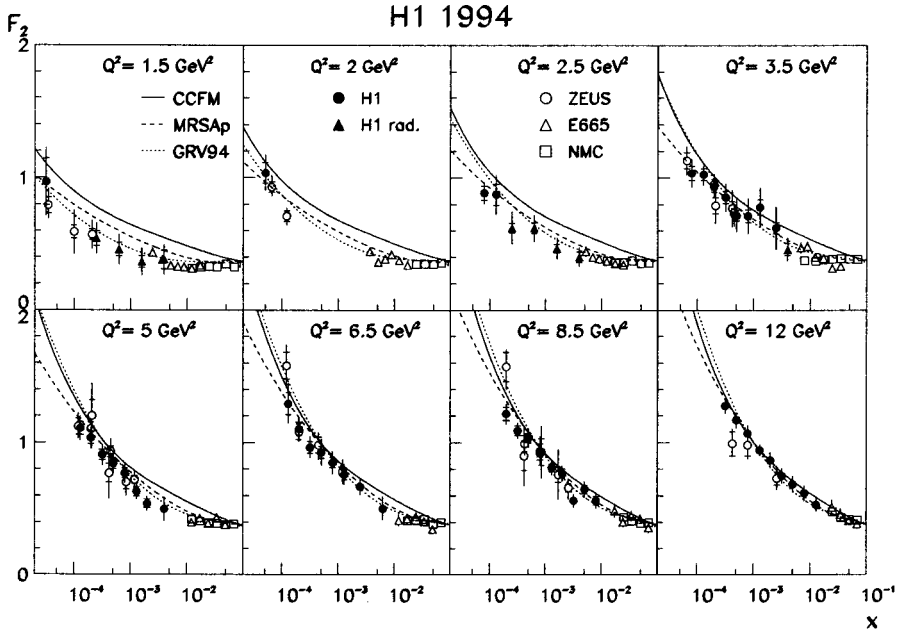

Fig. 7. Measurement of the proton structure function $F_2(x, Q^2)$ in the low Q^2 region by H1, ZEUS, E665 and NMC (as in Fig. 6). The solid lines are a prediction of the CCFM calculation. The GRV and MRSA′ curves are the same as in Fig. 6 and given for comparison.

A few different parametrizations are shown in Fig. 7 and Fig. 8. The first one shows the predictions using instead of the DGLAP equations the CCFM equations [20, 21], based on angular ordering. These go beyond the $\log Q^2$ approach and effectively include part of the $\log 1/x$ terms. Hence the small x behaviour of F_2 can be predicted. Except for the lowest Q^2 bins they are in good agreement with the data. Improvements to these calculations

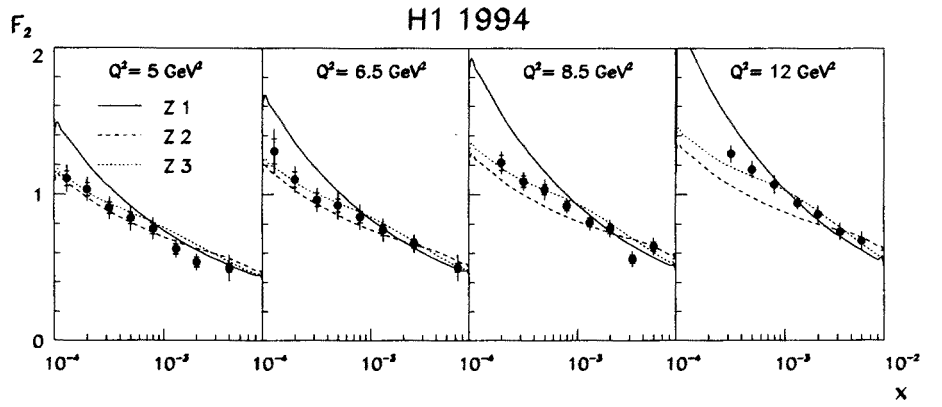

Fig. 8. Measurement of the proton structure function $F_2(x, Q^2)$ in the Q^2 region from 5 to 12 GeV^2 by H1. The curves are calculations of F_2 with no shadowing (Z1) and with weak (Z3; $R = 3\text{GeV}^{-1}$) and strong (Z2; $R = 2\text{GeV}^{-1}$) shadowing terms.

were recently made, taking into account the limited phase space [22]. In Fig. 8 some predictions [23] are shown using a previous version of the GRV model (Z1) and adding shadowing terms in the evolution using the GLR [24] equation (Z2,Z3). This follows the idea that at small x the parton densities become so large that annihilation and recombination of parton pairs could compete with the parton decay processes included in the standard evolution equations. The calculations are made for a strong ($R = 2\text{GeV}^{-1}$; hotspot) and weak ($R = 3\text{GeV}^{-1}$) shadowing scenario, starting at $x = 10^{-2}$. Here R is the recombination strength parameter in the GLR equation. It was observed that restoring the momentum sum rule in the GLR equation introduces additional "anti-shadowing" terms which will reduce the shadowing effect in the HERA regime.

Figs. 4 and 5 show that the GRV gives a good description of the data in the whole Q^2 range. The success of the GRV approach suggests that the observed rise of the structure function F_2 towards low x is generated by QCD dynamics. This was already noticed in 1974 [25] from a study of the behaviour of F_2 in the limit of large Q^2 and low x. In this asymptotic region the QCD evolution determines the shape of F_2. Recently Ball and Forte [26] developed a convenient way to test the asymptotic behaviour of F_2 using two variables

$$\sigma \equiv \sqrt{\log(x_0/x) \cdot \log(\alpha_s(Q_0)/\alpha_s(Q))}\,, \quad \rho \equiv \sqrt{\frac{\log(x_0/x)}{\log(\alpha_s(Q_0)/\alpha_s(Q))}}\,, \quad (6)$$

where $\alpha_s(Q)$ is evaluated at the two loop level [27].

The parameters x_0 and Q_0^2 have to be determined experimentally. The parameter Q_0^2 is optimized by minimizing the χ^2 of a linear fit of $\log(R'_F F_2)$ versus σ (see below) using data with $Q^2 \geq 5$ GeV^2. This leads to a value of $Q_0^2 = 2.5$ GeV^2. The same procedure was followed for x_0, which showed less sensitivity. The value $x_0 = 0.1$, as suggested in [26, 29], was found to be a good choice. To visualize the double scaling, it was proposed to rescale F_2 with factors R'_F and R_F defined as

$$R_F(\sigma,\rho) = 8.1 \exp\left(-2\gamma\sigma + \omega\frac{\sigma}{\rho} + \tfrac{1}{2}\log(\gamma\sigma) + \log\left(\frac{\rho}{\gamma}\right)\right)/\xi_F \qquad (7)$$

with

$$\xi_F = 1 + ((\xi_1 + \xi_2) * \alpha_s(Q) - \xi_1 * \alpha_s(Q_0)) * (\rho/(2\pi * \gamma)) \qquad (8)$$

and

$$R'_F(\sigma,\rho) = R_F \exp(2\gamma\sigma)\,. \qquad (9)$$

Here $\xi_1 = (206n_f/27 + 6b_1/b_0)/b_0$, $\xi_2 = 13$, $b_0 = 11 - 2n_f/3$, $\omega = (11 + 2n_f/27)/b_0$ and $b_1 = 102 - 38n_f/3$. The number of flavours is n_f and $\gamma = \sqrt{(12/b_0)}$. The function $\log(R'_F F_2)$ is then predicted to rise linearly with σ. $R_F F_2$ is expected to be independent of ρ and σ. Note that these expectations are valid only if the gluon distribution, which drives F_2 at low x via the sea quarks, does not have a too singular behaviour for $Q^2 = Q_0^2$.

Fig. 9a shows $R_F F_2$ versus ρ for the data with $Q^2 \geq 3.5$ GeV^2. The value of Λ for four flavours was chosen to be 263 MeV [28]. Approximate scaling is observed for $Q^2 \geq 5$ GeV^2 and $\rho \geq 2$. At high ρ the low Q^2 data tend to violate the scaling behaviour which is seen clearly for the data at 3.5 GeV^2.

In Fig. 9b, the results are shown for $\rho \geq 2$ and $Q^2 \geq 5$ GeV^2 as a function of σ. The data exhibit the expected linear rise of $\log(R'_F F_2)$ with σ. A linear fit to the data gives a value for the slope of: $2.50 \pm 0.02 \pm 0.06$ ($2.57 \pm 0.05 \pm 0.06$) for $Q^2 < 15$ GeV^2 ($Q^2 > 35$ GeV^2) and 4 (5) flavours. The first error is the statistical error and the second error is the systematic error taking into account the point-to-point correlations. The value expected from QCD is 2.4 (2.5) for 4 (5) flavours. The results are in agreement with these predictions. Not included in this error is the influence of the uncertainty in the choice of Λ. Varying Λ by $\pm$65MeV changes the result on the slope by ∓ 0.03.

One can conclude that the low x, low Q^2 measurements for $Q^2 \geq 5$ GeV^2 show scaling in ρ and σ. Thus double asymptotic scaling is a dominant feature of F_2 in this region leaving little need for other contributions.

Both the H1 and ZEUS experiments have performed next-to-leading order (NLO) QCD fits based on the DGLAP evolution equations on the

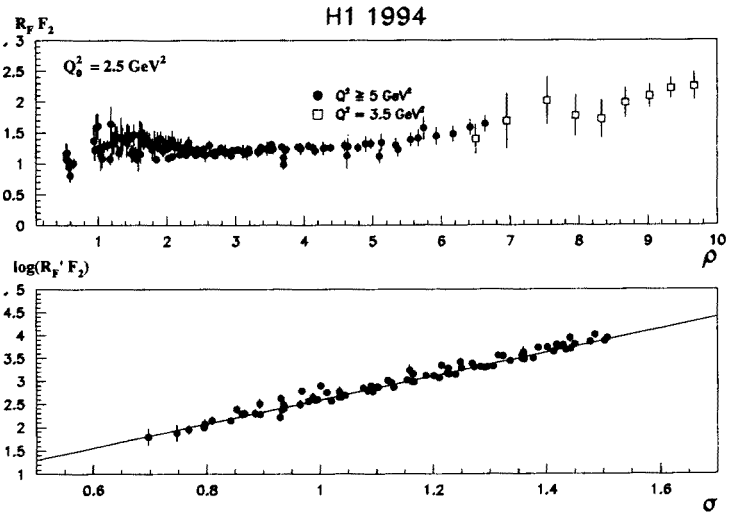

Fig. 9. The rescaled structure functions a) $R_F F_2$ versus ρ and b) $\log(R_F' F_2)$ *versus* σ (see text). Only data with $Q^2 \geq 5$ GeV^2 and $\rho > 2$ are shown in b).

HERA and fixed-target F_2 data. The curve in Fig. 3 shows that the F_2 data can be well described by such a QCD fit. Note that only data with $Q^2 \geq 5$ GeV^2 were used in the fit. The fit result was evolved to lower Q^2 and used as a prediction in the region $Q^2 < 5$ GeV^2. The low Q^2 data are found to be well described. This result suggests that, within the present accuracy, no (large) higher twist terms are required in this region. This may need to be reviewed when higher precision data at low x become available. In conclusion, as was anticipated from the comparison with DGLAP based predictions and from the asymptotic scaling of the data, partons satisfying the conventional DGLAP [3] evolution seem to be well able to describe the new HERA and fixed-target deep inelastic data down to as low as $Q^2 \sim 1$ GeV^2. Note however that, as discussed in [29], a similar quality fit can be obtained by using the BFKL evolution equations for the gluon. Hence both approximations can give a consistent description of the data within its present precision, but as yet there is no evidence that the $\ln 1/x$ terms play an important role in the HERA regime. This discussion will be continued in Section 5.

Assuming the DGLAP is the correct underlying evolution, the scaling violations from the HERA data allow an estimate of the gluon density $xg(x)$ at low values of x. Data from the fixed-target experiments are needed to constrain the high x region. The H1 QCD fit [29] based on the 1993 F_2 data includes only proton data from H1, NMC and BCDMS. Additionally the momentum fraction carried by the gluon is imposed to be 0.44. Apart

from the 1993 ZEUS data, the ZEUS QCD fit [30] includes data from NMC, both on proton and deuteron targets. The results are shown in Fig. 10a for $Q^2 = 20$ GeV^2. The error bands shown include a careful analysis of the systematics, taking into account the correlation between different sources. The results of the two experiments agree very well. The resulting gluon distribution shows a clear rise with decreasing x. Similar results have been found in [16], which include also other data than those from structure functions. In the region $x > 10^{-2}$ the extracted gluon densities agree with the result obtained by the NMC.

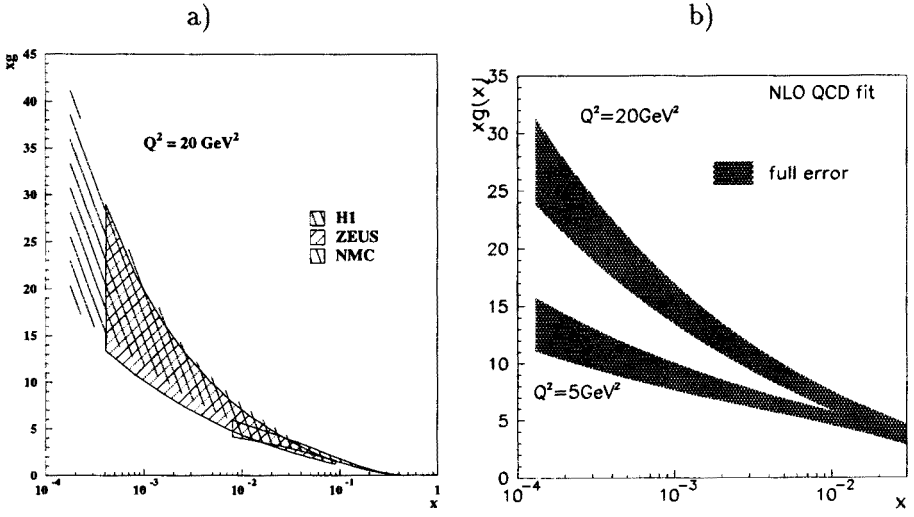

Fig. 10. a) The gluon density $xg(x)$ at 20 GeV^2 based on the 1993 data samples, extracted from NLO QCD fits by the H1 [29], ZEUS [30] and NMC [31] Collaborations.b) The gluon density $xg(x)$ at 5 GeV^2 and 20 GeV^2 based on the 1994 data samples, extracted from a NLO QCD fit by the H1 [4].

In Fig. 10b the new result of H1 is shown, based on the 1994 data. The fit now also includes NMC and BCDMS deuteron data, and there is no constraint on the momentum fraction carried by the gluon for this result. Details on this analysis are given in [4]. The error band is determined as before, apart from the effect of Λ_{QCD}. The latter was chosen to be 263 MeV, and a variation of 65 MeV produces a change on the gluon of 9% at 20 GeV^2. Due to the new data the precision of the gluon determination improved with a factor two in the low x region.

4. The charm contribution to F_2

A measurement of the contribution of F_2 which arises from charm production, $F_2^{c\bar{c}}$ has been advocated as a sensitive probe of the gluon density. It was recently [32] shown that at small x the fixed order QCD predictions are stable, with scale variations of less than $\pm 10\%$, and that they offer a rather local measurement of the gluon.

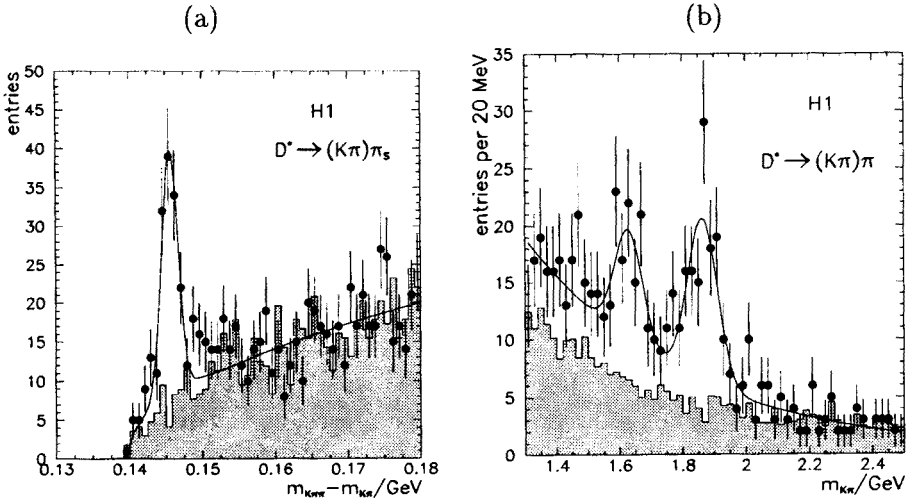

Fig. 11. Preliminary: distribution of (a) the mass difference $\Delta m = m(K^-\pi^+\pi^+_{\rm slow}) - m(K^-\pi^+)$ and (b) of the $K\pi$ mass for deep inelastic scattering events. The data points in the Δm distribution are obtained from the $m(K^-\pi^+)$ mass combinations within an interval of 90 MeV around the nominal D^0 mass. The shaded histogram shows the background expectation, which is obtained from the high mass sideband 2.0 GeV $\leq m(K^-\pi^+) \leq$ 2.6 GeV, normalized to the region 0.160 GeV $\leq \Delta m \leq$ 0.180 GeV. The solid line is a fit of two Gaussian plus the two body phase space distribution to the data as described in the text. The data points in the $K\pi$ mass distribution are obtained from a Δm interval of 2.2 MeV around the nominal D^{*+} position. The shaded histogram shows the background expectation from the region 0.170 GeV $\leq \Delta m \leq$ 0.180 GeV, normalized by the two body phase space factors according to the Δm intervals. The solid line represents the fit of two Gaussians for the D^0 and S^0 plus an exponential to the data.

H1 presents preliminary measurements of $F_2^{c\bar{c}}$. Events with charm are tagged through the detection of D^0 and $D^{*\pm}$ mesons. The decays $D^0 \to K^-\pi^+$ and $D^{*+} \to D^0\pi^+ \to K^-\pi^+\pi^+$ (and charge conjugate channels) have been analysed. Mass plots for the D^* signal are shown in Fig. 11. The latter was analysed making use of the "slow pion" method. The data contain $104 \pm 12\, D^*$ and $144 \pm 19\, D^0$ candidates above background, for $Q^2 > 10$ GeV^2 and a luminosity of about 3 pb^{-1}. Details of this analysis are given

in [33]. There it is also demonstrated that the production mechanism for charm in DIS is compatible with being photon-gluon fusion. Hence $F_2^{c\bar{c}}$ will indeed be useful as a direct probe of the gluon density in the proton. The present level of precision of the data does not allow yet the extraction of the gluon from the $F_2^{c\bar{c}}$ data.

The charm contribution $F_2^{c\bar{c}}(x, Q^2)$ to the structure function is derived from the one photon exchange cross section for charm production

$$\frac{d^2\sigma^{c\bar{c}}}{dxdQ^2} = \frac{4\pi\alpha^2}{Q^4 x}\left(1 + (1-y)^2\right) F_2^{c\bar{c}}(x, Q^2)\,, \tag{10}$$

with the simplification that the Callan-Gross relation holds, *i.e.* $R = F_2/2xF_1 - 1 \equiv 0$. The effect of R is small in the present region, in particular in comparison with the measurement precision on $F_2^{c\bar{c}}$

The charm contribution to the proton structure function is obtained from the numbers of reconstructed D^{*+} and D^0 mesons which are converted to bin averaged cross sections based on the Monte Carlo efficiency calculation. For the latter the program AROMA [34] has been used. The kinematics is calculated from the electron information (Eq. 3). The resolution in x is roughly 14% at small x and 30% at large x. Higher order QED corrections are applied using the program HECTOR [35].

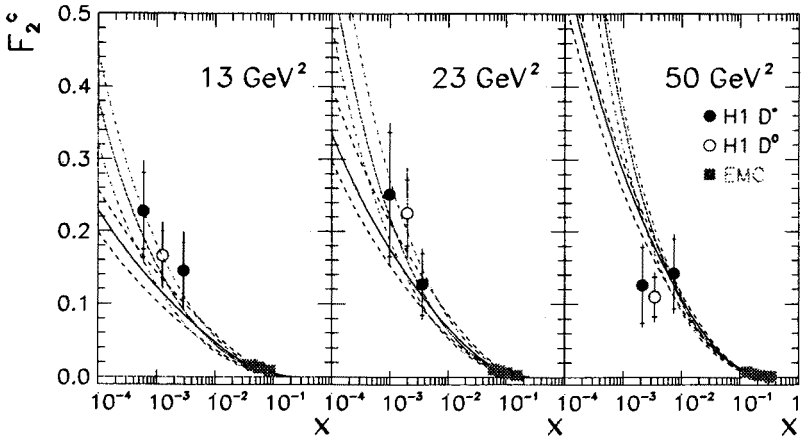

Fig. 12. Preliminary: the charm contribution $F_2^{c\bar{c}}$ to the proton structure function as derived from the inclusive D^{*+} (full dots) and D^0 analysis (open circles) in comparison with the NLO calculations based on the GRV-HO (upper lines) and CTEQ2MF (lower lines). The full lines give the predictions for $m_c = 1.5$ GeV while the dashed lines indicate the changes for $m_c = 1.3$ GeV (upper dashed lines) and $m_c = 1.7$ GeV (lower dashed lines). The EMC data are also shown (full boxes).

In Fig. 12 the results of the $F_2^{c\bar{c}}$ measurements are displayed, both for D^0 and D^* meson production. The error refers to the statistics and to the experimental systematics. Systematics include the uncertainty on the branching rations, the $c \to D$ ratio, event and track selection efficiencies and acceptances, and background uncertainties. An error of 10% due the determination procedure of the inclusive D meson yield per bin and a kinematics dependent error due to the energy and angular resolution of the electron measurement have been included as well. On top of these errors there is an overall normalization uncertainty in the cross section of 12%(11%) in case of the D^0 (D^{*+}) analysis due to the error in $B(c \to D^0)$ and $B(c \to D^{*+})$.

The measurement at HERA extends the knowledge on $F_2^{c\bar{c}}$ by two orders of magnitude towards smaller x values for the measurements by the EMC experiment [36]. Together with this early measurement a steep rise of $F_2^{c\bar{c}}$ is observed with decreasing x. The data are also compared with the NLO calculations [32] based the GRV and CTEQ2MF [37] parameterization of the gluon density in the proton. The calculations are in good agreement with the data. The dominant uncertainty in the QCD calculations arises from the uncertainty in the charm quark mass.

5. Search for BFKL signatures in hadronic final states

In order to make further progress to find the appropriate QCD approach to use in the small x regime, hadronic final states are analysed. The experiments at HERA measure the full hadronic final state, apart from losses in the beam pipe. In this section we will discuss some recent measurements aiming to detect the onset of QCD $\alpha_S \log 1/x$ resummation effects, complementary to the structure function studies.

For events at low x, hadron production in the region between the current jet and the proton remnant is expected to be sensitive to the effects of the BFKL or DGLAP dynamics. At lowest order the BFKL and DGLAP evolution equations effectively resum the leading logarithmic $\alpha_S \ln 1/x$ and $\alpha_S \ln Q^2$ contributions respectively. In an axial gauge this amounts to a resummation of ladder diagrams of the type shown in Fig. 13. This shows that before a quark is struck by the virtual photon, a cascade of partons may be emitted. The fraction of the proton momentum carried by the emitted partons, x_i, and their transverse momenta, k_{Ti}, are indicated in the figure. In the leading $\log Q^2$ DGLAP scheme this parton cascade follows a strong ordering in transverse momentum $k_{Tn}^2 \gg k_{Tn-1}^2 \gg ... \gg k_{T1}^2$, while there is only a soft (kinematical) ordering for the fractional momentum $x_n < x_{n-1} < ... < x_1$. In the BFKL scheme the cascade follows a strong ordering in fractional momentum $x_n \ll x_{n-1} \ll ... \ll x_1$, while there is no ordering in transverse momentum. The transverse momentum follows a

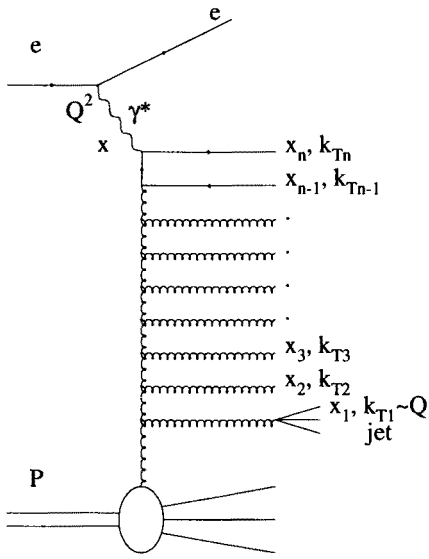

Fig. 13. Parton evolution in the ladder approximation. The selection of DIS events containing a forward jet is illustrated.

kind of random walk in $\log k_T$ space: the value of k_{Ti} is close to that of k_{Ti-1}, but it can be both larger or smaller.

Several measurements of the hadronic final state have been suggested to exploit this difference at the parton level. The idea is to find observables which may reflect both of the BFKL characteristics of the unintegrated gluon distribution $f(x, k_T^2)$, that is the $x^{-\lambda}$ growth and the diffusion in $\log k_T^2$, as x decreases. Here we discuss the transverse energy (E_T) flow in the region away from the current quark jet and second, and the distribution of deep inelastic events containing an identified forward jet, that is, a measured jet as close as possible to, but distinct from, the proton remnants. Apart from numerical calculations, predictions for final state observables are also available as Monte Carlo models, based upon QCD phenomenology. The CDM [38] model description of gluon emission is similar to that of the BFKL evolution, because the gluons emitted by the dipoles do not obey strong ordering in k_T [39]. The CDM does not explicitly make use of the BFKL evolution equation, however. The MEPS [40] model is based on DGLAP dynamics; the emitted partons generated by the leading log parton showers are strongly ordered in k_T.

Due to the absence of k_T ordering the BFKL approach is expected to give a larger transverse energy, E_T, in the hadronic final state in the central region of the hadronic centre-of-mass than the DGLAP approach at low x. This corresponds to the very forward region of the detectors in the

HERA laboratory frame. In this central region of the hadronic center-of-mass Golec-Biernat *et al.*, , [41] show using the DGLAP approach that the partonic mean E_T, $\langle E_T \rangle$, increases with increasing x, while for BFKL the reverse is true, $\langle E_T \rangle$ decreases with increasing x. It should be noted though that the E_T spectra are difficult to calculate in the DGLAP framework because the E_T weighting emphasizes unsafe regions of phase space.

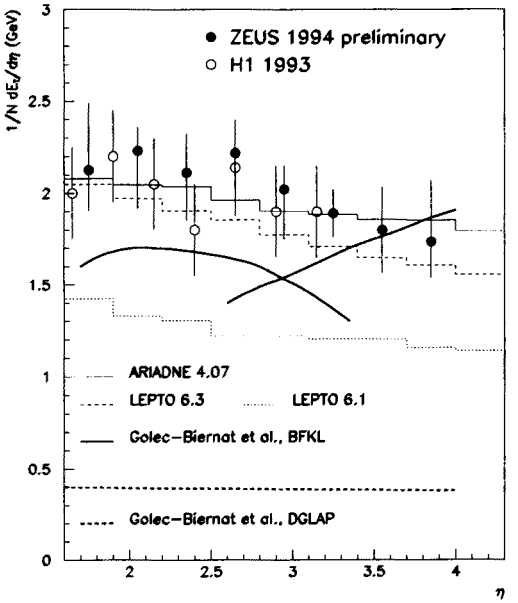

Fig. 14. Mean transverse energy per unit rapidity in the forward region of the HERA lab. system.

Fig. 14 shows the transverse energy flow as a function of pseudorapidity, η, in the laboratory frame as measured by both H1 [42] and ZEUS [43]. The level of E_T is almost flat at ~ 2 GeV/(unit of η). Also shown are the partonic calculations from [41] which seem to indicate a preference towards the BFKL approach over DGLAP. In order to investigate hadronisation effects in this region two Monte Carlo generators have been studied: the CDM model (labeled ARIADNE 4.07 on the figure) and LEPTO 6.1, both of which are based on the Lund string fragmentation framework. The data shown in Fig. 14 are reasonably described by CDM, whereas the overall E_T predicted by LEPTO 6.1 is far too low. Unfortunately this version of LEPTO is very sensitive to the cut-off applied to avoid divergences in the matrix element — the boson-gluon-fusion (BGF) process, which is the dominant $\mathcal{O}(\alpha_S)$ graph at low Q^2 and x, creates two Lund strings as opposed to only one from the QCD Compton process or a $\mathcal{O}(\alpha_S^0)$ scattered quark. The

effect of the presence of strings is an increased amount of E_T available in the hadronisation phase. A newer version of the program, LEPTO 6.3, reduced this dependence on the matrix element cut-off by treating the scattering off a sea quark in a manner similar to the 2 string scenario of the BGF case. Using this version of the generator allows a better description of the data, though there are still some problems in describing the x dependence in the lowest Q^2 region. However, the measurement seems to be rather sensitive to the non-perturbative hadronisation phase and can, in its present form, no longer be considered as a direct sensitive test of BFKL dynamics.

Another possible signature of the BFKL dynamics is the behaviour of deep inelastic (x, Q^2) events which contain a measured jet (x_j, k_{Tj}^2) in the kinematic regime where $k_{Tj}^2 \simeq Q^2$ (so as to neutralise the ordinary gluon radiation which would have arisen from DGLAP evolution) and where the jet has longitudinal momentum fraction x_j as large as is experimental feasible ($x_j \sim 0.1$). The aim is to observe events with x/x_j as small as possible. According to BFKL dynamics the differential structure function has a leading small x/x_j behaviour of the form [44]

$$x_j \frac{\partial F_2}{\partial x_j \partial k_{Tj}^2} \sim \alpha_S(k_{Tj}^2)\, x_j \left[g + \frac{4}{9}(q+\overline{q})\right] \left(\frac{x}{x_j}\right)^{-\lambda},$$

where the parton distributions are to be evaluated at (x_j, k_{Tj}^2) — where they are well known from global analyses. The idea is to see if the DIS + forward jet data show evidence of the $(x/x_j)^{-\lambda}$ behaviour. Jets are generally expected to be more robust against hadronisation effects than is the E_T flow. H1 has studied DIS events at small x which have a jet with large x_j. A cone algorithm is used to find jets, requiring an E_T larger than 5 GeV in a cone of radius $R = \sqrt{\Delta\eta^2 + \Delta\phi^2} = 1.0$ in the space of pseudo-rapidity η and azimuthal angle ϕ in the HERA frame of reference. In order not to confuse the forward jet with the one at the top of the ladder the requirement $y > 0.1$ was imposed to ensure that the jet of the struck quark is well within the central region of the detector and is expected to have a jet angle larger than 60°. Experimentally a cone algorithm is used to find jets, requiring an E_T larger than 5 GeV in a cone of radius $R = \sqrt{\Delta\eta^2 + \Delta\phi^2} = 1.0$ in the space of pseudo-rapidity η and azimuthal angle ϕ in the HERA frame of reference. Jets are accepted as forward jets if $x_j > 0.025$, $0.5 < k_{Tj}^2/Q^2 < 4$, $6° < \theta_j < 20°$ and $k_{Tj} > 5$ GeV, where θ_j is the forward jet angle and k_{Tj} is the transverse momentum of the jet. These selection criteria allow a study the cross section of forward jet production in the region $Q^2 \sim 20$ GeV^2 and $2{\cdot}10^{-4} < x < 2{\cdot}10^{-3}$. Hence the ratio x_j/x is always larger than 10.

TABLE I

Numbers of observed DIS events with a selected forward jet, corrected for radiative events faking this signature. These may be directly compared with the expectations from the Monte Carlo models. The measured cross section $ep \to \text{jet}+X$ for forward jets is also given. The errors reflect the statistical and systematic uncertainties.

x range	data events	MEPS events	CDM events	$\sigma(ep \to \text{jet}+X)$ (pb)
$2 \cdot 10^{-4} - 1 \cdot 10^{-3}$	271	141	282	$709 \pm 42 \pm 166$
$1 \cdot 10^{-3} - 2 \cdot 10^{-3}$	158	101	108	$475 \pm 39 \pm 110$

The resulting number of events observed with at least one forward jet in the kinematical region $160° < \theta_e < 173°$ and $E_e > 12$ GeV is given in Table I and compared to expectations of the MEPS and CDM models after detector simulation and corrected for background. The measured cross section for forward jets satisfying the cuts given above is also presented in Table I. It has been corrected for detector effects using the CDM. The ratio of the jet cross section for the low x to the high x bin is 1.49 ± 0.25.

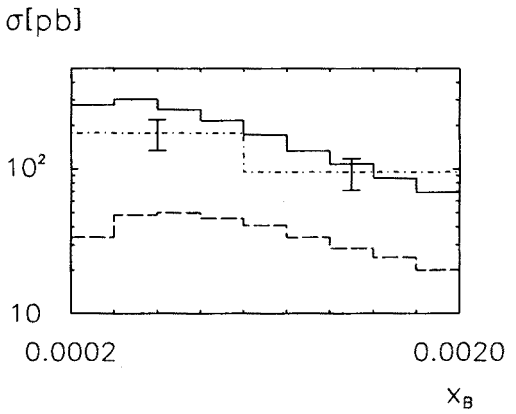

Fig. 15. Comparison of the BFKL calculation and the approximate analytical calculation of the three-parton matrix elements, compared with the data of the H1 experiment.

In Fig. 15 the data are compared with a recent calculation [45]. The calculation (at the parton level) has exactly the same cuts as the measurement. The solid line is a BKFL calculation, while the dashed line is an approximate analytical three-parton matrix element calculation without the BFKL ladder. The results of H1 are compared with the calculations. The BFKL curve agrees well with the data, while the lower curve is in clear disagreement. Several corrections to this result should be considered, as discussed

in [45] (*i.e.* the calculation is at the parton level while the data are at the hadron level). Nevertheless the agreement with data is encouraging and such measurements should be explored further with larger statistics event samples as they have a large potential to reveal BFKL effects in the data.

A final general comment is in order. The smaller the value of x/x_j the larger is the BFKL effect and the more dominant is the leading $\log(1/x)$ formalism. As with all BFKL predictions, the reliability can only be quantified when the sub-leading corrections are known. Moreover by measuring properties of the final state we inevitably reduce the "reach" of HERA. For example in the present case we require x/x_j to be as small as possible, yet experimentally jet recognition demands $x_j \approx 0.1$, so we lose an order of magnitude in "reaching small x".

6. Summary

The structure function studies at HERA have made impressive progress in the last year. The new kinematical range covered is $1.5\ \mathrm{GeV}^2 < Q^2 < 5000\ \mathrm{GeV}^2$ and $3 \cdot 10^{-5} < x < 0.32$. The rise of the structure function is confirmed with high precision and persists even in the lowest accessible Q^2 region. For $Q^2 \geq 5\ \mathrm{GeV}^2$, the data exhibit double asymptotic scaling, suggesting that the observed rise of the structure function towards low x is generated by QCD dynamics. The data are indeed well described by a Next-to-Leading Order (DGLAP) QCD fits; no evidence for the presence of BFKL effects in F_2 has been demonstrated yet. The complementary information from the hadronic final states will be required to shed more light on this question.

I thank the organizers for the invitation to this interesting conference. I also wish to thank J. Dainton, K. Daum, M. Lancaster, G. Rädel and P. Sutton for discussion, and valuable help with some of the figures.

REFERENCES

[1] A. De Roeck, *J. Phys.* **G19**, 1549 (1993).
[2] BFKL: E.A. Kuraev, L.N. Lipatov, V.S. Fadin, *Phys. Lett.* **B60**, 50 (1975); *Sov. Phys. JETP* **44**, 443 (1976); *Sov. Phys. JETP* **45**, 199 (1977); Ya.Ya. Balitsky, L.N. Lipatov, *Sov. J. Nucl. Phys.* **28**, 822 (1978).
[3] DGLAP: V.N. Gribov, L.N. Lipatov, *Sov. J. Nucl. Phys.* **15**, 438 (1972); G. Altarelli, G. Parisi, *Nucl. Phys.* **B126**, 298 (1977); Yu.L. Dokshitzer, *Sov. Phys. JETP* **46**, 641 (1977).
[4] H1 Collaboration: S. Aid *et al.*, DESY preprint, 96-039 (1996).
[5] ZEUS Collaboration: M. Derrick *et al.*, *Z. Phys.* **C69**, 607 (1996).

[6] F. Eisele, Proc. of Int. Europhysics Conf. on HE Physics, Brussels, 1995. DESY preprint 95-229. A. Caldwell, Proceedings of the 1995 International Symposium on Lepton and Photon Interactions at High Energies, Beijing, DESY-95-231.
[7] G. Altarelli, G. Martinelli, *Phys. Lett.* **B76**, 89 (1978).
[8] S. Bentvelsen, P. Kooijman, J. Engelen, Proc. of the Workshop *Physics at HERA*, ed. W. Buchmüller, G. Ingelman, Hamburg 1992, p.23; K.C. Hoeger, Proceedings of the Workshop *Physics at HERA*, ed. W. Buchmüller and G. Ingelman, Hamburg 1992, p.43.
[9] H1 Collaboration: T. Ahmed *et al.*, *Nucl. Phys.* **B439**, 471 (1995).
[10] U. Bassler, G. Bernardi, DESY preprint 94-231 (1994), submitted to *Nucl. Inst. Meth.*
[11] P. Kooijman, Talk at the Workshop DIS95, Roma (1996).
[12] NMC: M. Arneodo *et al.*, *Phys. Lett.* **B364**, 107 (1995).
[13] BCDMS Collaboration: A. C. Benvenuti *et al.*, *Phys. Lett.* **B223**,485 (1989); **B237**,592 (1990).
[14] E665 Collaboration, M.R. Adams *et al.*, FNAL-Pub-95/396-E (1995).
[15] M. Glück, E. Reya, A. Vogt, *Z. Phys* **C67**, 433 (1995).
[16] A.D. Martin, R.G. Roberts, W.J. Stirling, *Phys. Lett.* **B354**, 155 (1995).
[17] CTEQ Collaboration: H.L. Lai *et al.*, *Phys. Rev.* **D51**, 4763 (1995).
[18] A. Donnachie, P.V. Landshoff, *Z. Phys.* **C61**, 139 (1994).
[19] A. Capella *et al.*, *Phys. Lett.* **B337**, 358 (1994). For this calculation the intercept $1 + \delta$ was taken with $\delta = 0.25$ and no QCD evolution was used in the region shown.
[20] M. Ciafaloni, *Nucl. Phys.* **B296**, 49 (1988); S. Catani, F. Fiorani, G. Marchesini, *Phys. Lett.* **B234**, 339 (1990); *Nucl. Phys.* **B336**, 18 (1990).
[21] J. Kwiecinski, A.D. Martin, P.J. Sutton, Durham DTP/95/94.
[22] J. Kwiecinski, A.D. Martin, P.J. Sutton, Durham preprint DTP/96/02.
[23] Wei Zhu, Kang-Min Chai, Bo He, *Nucl. Phys.* **B449**, 183 (1995).
[24] V.N. Gribov, E.M. Levin, M.G. Ryskin, *Phys. Rep.* **100**, 1 (1983).
[25] A. De Rújula *et al.*, *Phys. Rev.* **D10**, 1649 (1974).
[26] R.D. Ball, S. Forte, *Phys. Lett.* **B335**, 77 (1994).
[27] R.D. Ball, S. Forte, *Acta Phys. Pol.* **26B**, 2097 (1995).
[28] M. Virchaux, A. Milsztajn, *Phys. Lett.* **B274**, 221 (1992).
[29] H1 Collaboration: S. Aid *et al.*, *Phys. Lett.* **B354**, 494 (1995).
[30] ZEUS Collaboration: M. Derrick *et al.*, *Phys. Lett.* **B345**, 576 (1995).
[31] NMC: M. Arneodo *et al.*, *Phys. Lett.* **B309**, 222 (1993).
[32] A. Vogt, DESY preprint 96-012 (1996).
[33] K. Daum, Talk at the Workshop DIS95, Roma (1996).
[34] G. Ingelman, G.A. Schuler,Proc. of the Workshop on Physics at HERA, Hamburg 1991, eds. W. Buchmüller, G. Ingelman, vol. 3, p. 1346.
[35] A. Arbuzov *et al.*, DESY preprint 95-185 (1995).
[36] EMC Collaboration J.J. Aubert *et al.*, *Nucl. Phys.* **B213**, 31 (1983).
[37] W.K. Tung, Proceedings of the International Workshop on Deep Inelastic Scattering and Related Subjects, Eilat, Israel (1994).
[38] L. Lönnblad, *Comput. Phys. Commun.* **71**, 15 (1992).

[39] L. Lönnblad, *Z. Phys.* **C65**, 285 (1995); A.H. Mueller, *Nucl. Phys.* **B415**, 373 (1994); L. Lönnblad, Proc. of PHOTON'95, Sheffield, 1995, eds. D.J. Miller, S.L. Cartwright and V.A. Khoze, p. 443.

[40] G. Ingelman, Proc. of the Workshop on Physics at HERA, Hamburg 1991, eds. W. Buchmüller and G. Ingelman, vol. 3, p. 1366.

[41] K. Golec-Biernat, J. Kwieciński, A.D. Martin, P.J. Sutton, *Phys. Lett.* **B335**, 220 (1994); *Phys. Rev.* **D50**, 217 (1994).

[42] H1 Collaboration: S. Aid *et al.*, *Phys. Lett.* **B356**, 118 (1995).

[43] ZEUS Collaboration: Proc. of Int. Europhysics Conf. on HE Physics, Brussels, 1995. Ref. 0391.

[44] A.H. Mueller, *Nucl. Phys. B (Proc. Suppl.)* **18C**, 125 (1990); *J. Phys.* **G17**, 1443 (1991); J. Kwieciński, A.D. Martin, P.J. Sutton, *Phys. Rev.* **D46**, 921 (1992); *Phys. Lett.* **B287**, 254 (1992); *Nucl. Phys. B (Proc. Suppl.)* **29A**, 67 (1992); J. Bartels, A. De Roeck, M. Loewe, *Z. Phys.* **C54**, 635 (1992); *Nucl. Phys. B (Proc. Suppl.)* **29A**, 61 (1992); W.K. Tang, *Phys. Lett.* **B278**, 363 (1992).

[45] J. Bartels *et al.*, DESY preprint 96-036.